

Effect of Heat Treatment on Fracture Toughness of As-Forged AZ80 Magnesium Alloy

Min Deng, Hui-Zhong Li, Si-Nan Tang, Hui-Juan Liao, Xiao-Peng Liang, and Ruo-Mei Liu

(Submitted December 2, 2014; in revised form March 12, 2015; published online March 31, 2015)

The effect of heat treatment on the plane-strain fracture toughness in forged AZ80 magnesium alloy was studied. Two different kinds of heat treatment technologies (T5 and T6) were performed on the forged samples. The values of plane-strain fracture toughness (K_{IC}) were obtained from the stretched zone (SZ for short) analysis. The results showed that the as-forged specimen would produce a large quantity of β -Mg₁₇Al₁₂ precipitates both in the interior of the grains and at grain boundaries after T5 and T6 heat treatments. The β -Mg₁₇Al₁₂ displayed a precipitation strengthening. Compared with the as-forged specimen, the ultimate tensile strengths of T5 and T6 specimens were improved by 42.8 and 30 MPa, respectively. And the K_{IC} of T5 and T6 specimens also increased to 23.8 and 21.0 MPa m^{1/2} while that of the as-forged sample was 17.9 MPa m^{1/2}. The average grain size of T5 sample was similar to that of the as-forged one, but was finer than that of T6 specimen. The best mechanical properties and fracture toughness of forged AZ80 magnesium alloy were achieved after T5 treatment.

Keywords AZ80 magnesium alloy, fracture toughness, heat treatment, precipitates

1. Introduction

In recent years, magnesium alloys have attracted a lot of interest for structural applications in automotive and aerospace industries due to their low density and high strength-to-weight ratio (Ref 1-4). When they are used in structural applications, their mechanical properties must satisfy reliability and safety requirement. One of the methods of ensuring that is to study their fracture toughness. Several reports have been made about the fracture toughness in magnesium and magnesium alloys (Ref 5-9). Allowing for the value of fracture toughness in magnesium alloy is generally lower than that of aluminum alloy from the Ashby map (Ref 10), several researches have been carried out to improve the fracture toughness of magnesium alloys. Somekawa et al. (Ref 11-13) have demonstrated that the fracture toughness of magnesium alloys could be improved by grain refinement, equal-channel-angular extrusion, and texture. It also can be improved by controlling the shape of precipitates in ZK60 (Ref 14). Although these methods can improve the fracture toughness of magnesium and magnesium alloys, the effect of heat treatment is rarely studied. In addition, the method to measure the fracture toughness from ASTM-E399 is restricted to thick specimens and only few methods are reported to

evaluate the fracture toughness of thin samples. While, Spitzig (Ref 15) explained the relationship between stretched zone size and critical tip opening displacement (CTOD), and evaluated the value of fracture toughness. Furthermore, Sasaki et al. (Ref 16) applied the stretched zone (SZ for short) analysis method to evaluate the plane strain fracture toughness of thin magnesium alloys.

The AZ80 alloy has been a well-known commercial magnesium alloy due to its high strength and low price (Ref 17-19). Recently, studies on AZ80 alloy are mainly focused on the effect of processing method or heat treatment on its microstructures as well as its mechanical properties (Ref 20-22), creep behaviors (Ref 23), and corrosion (Ref 24). Moreover, the studies on fracture toughness in Mg-Al alloys are mainly concentrated on AZ31 alloy rather than deformed AZ80 alloy. Therefore, the effect of heat treatment on the fracture toughness of forged AZ80 magnesium alloy was studied in this paper, and the SZ analysis was applied to evaluate the fracture toughness.

2. Experimental Procedures

The experimental material was as-forged AZ80 magnesium plate with 280 mm diameter and 35 mm thickness. The chemical composition was Mg-8.2Al-0.55Zn-0.32Mn (wt.%). The as-forged plate was formed by die forging of a cylindrical billet. The initial thickness of billet was 75 mm, and the forging temperature was 693 K. All the specimens were cut at concentric circles position of as-forged plate. In this study, T5 and T6 heat treatments were carried out to obtain different microstructures. The solution treatment was performed at 693 K for 20 h followed by air cooling. Aging at 443 K for 20 h was performed using the as-forged and solution-treated specimens, i.e., T5 and T6 treatments, respectively.

The x-ray diffraction (XRD, D/Max 2500) was carried out at room temperature with Cu K α radiation, 40 kV tube voltages, and 30 mA current to identify the main phases of materials. The microstructure of the alloys was examined by optical microscopy (OM, Leica DMRX), scanning electron microscopy (SEM,

Min Deng, Si-Nan Tang, Hui-Juan Liao, and Ruo-Mei Liu, School of Materials Science and Engineering, Central South University, Changsha 410083, China; **Hui-Zhong Li**, School of Materials Science and Engineering, Central South University, Changsha 410083, China and State Key Laboratory of Powder Metallurgy, Central South University, Changsha 410083, China; and **Xiao-Peng Liang**, State Key Laboratory of Powder Metallurgy, Central South University, Changsha 410083, China. Contact e-mails: dmklp2013@163.com and lh2606@csu.edu.cn.

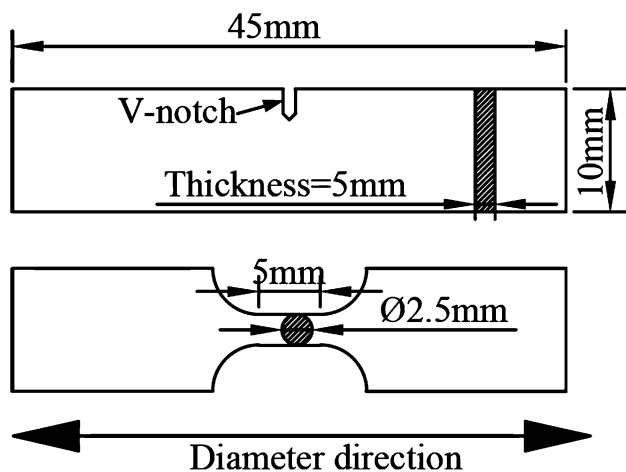


Fig. 1 Illustration of the sample cutting position

Sirion200), and transmission electron microscopy (TEM, JEM-2010). Specimens for OM and SEM were mechanically polished and chemically etched in a solution of 20 mL acetic acid + 1 mL HNO₃ + 60 mL ethylene glycol + 19 mL distilled water for 5-15 s. The TEM specimens were reduced to 0.06 mm thickness by hand, and then the foils were perforated by twin-jet polishing technique in a solution of 500 mL CH₃OH + 100 mL C₄H₁₄O₂ + 5.3 g LiCl + 11.16 g Mg(ClO₄)₂ at 243 K and 50 V.

Tensile tests were conducted on MTS810 universal material testing machine at room temperature. The initial strain rate was $1 \times 10^{-3} \text{ s}^{-1}$. Tensile specimens with a gage length of 5 mm and a gage diameter of 2.5 mm were machined from the forged materials. The tensile axis was selected to be parallel to the diameter direction.

Plane strain fracture toughness tests were carried out according to ASTM-E-399 (Ref 25) by MTS810 testing machine. The specimens were three-point bending samples 10 mm in width and 5 mm in thickness. The V-notch was normal to the diameter direction. Figure 1 shows the cutting position and dimensions of samples. Before fracture toughness test, fatigue crack test was performed to insert a fatigue pre-crack in the specimen, and the pre-crack length was between 0.45 and 0.55 W , where W was the width of the samples. The plane strain toughness tests were carried out with a cross-head speed of 1 mm/min at room temperature. In order to analyze the stretched zone, which was the trace of the blunt crack tip, the fracture surface after plane strain toughness test was examined by SEM and Wyko NT9100 optical surface profiler microscopy. The micro-hardness on the cross section after fracture toughness test was also measured by an HVS-1000 Vickers hardness tester. The applied load and holding time were 4.9 N and 15 s, respectively.

3. Results and Discussion

Figure 2 shows XRD patterns of as-forged, T5, and T6 specimens. Three phases were designated as α -Mg, β -Mg₁₇Al₁₂, and MgZn₂ from the results. The highest peak of β -Mg₁₇Al₁₂ could be found in T6 sample, followed by T5 sample and almost negligible amount of β -Mg₁₇Al₁₂ was observed in as-forged sample. There was no significant change of MgZn₂ observed after T5 and T6 treatments. This result

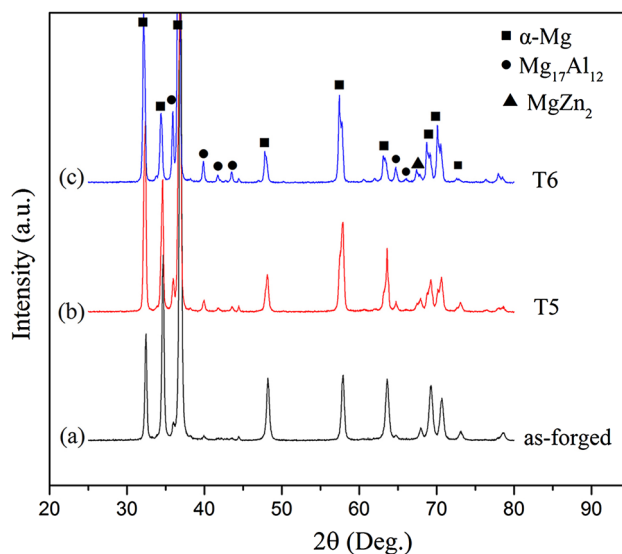


Fig. 2 XRD diffraction patterns of various AZ80 specimens

indicated that more β -Mg₁₇Al₁₂ appeared after T5 and T6 heat treatments.

The microstructures of specimens are revealed in Fig. 3(a)-(h). The left- and right-side figures in Fig. 3(a)-(f) depict the structures observed by optical microscopy and SEM, respectively. In this paper, all the average grain sizes were measured using the Image-Pro Plus 5.0 software with more than 1000 grains. Figure 3 shows the optical micrographs of as-forged (a), T5 (c), and T6 (e) specimens. The average grain sizes of the as-forged, T5, and T6 were measured to be 39.3, 40.3, and 46.1 μm , respectively. Compared to the as-forged specimen, the average grain size of T5 specimen was nearly unchanged after aging treatment, while the average grain size of T6 specimen grew up obviously. The main reason for this phenomenon was the high-temperature solution treatment during T6 treatment. These changes of grain size are in agreement with the results of previous studies. Chengling et al. (Ref 26) and Palai et al. (Ref 27) reported that the grain size of solution-treated sample was larger than that of the untreated sample. In addition, Yazhe et al. (Ref 28) reported that the grain size of AZ80 magnesium would grow up significantly after solution treatment at 698 K for 1-3 h. Figure 3 also shows the SEM micrograph of as-forged (b), T5 (d), and T6 (f) specimens. As shown in Fig. 3(b), only a few small precipitates are observed at grain boundaries. After heat treatment, a large quantity of precipitates were observed at the grain boundaries and in the interior of grains in Fig. 3(d) and (f). After calculating the precipitation regions in Fig. 3(d) and (f) with software, the region of precipitation was a litter wilder in T6 specimen than in T5 one. This might be caused by the decomposition of the super-saturated solid solution into β -Mg₁₇Al₁₂ and α -Mg during T6 treatment (Ref 29). Figure 3(g) and (h) shows the magnified views of precipitates in T5 and T6 specimens, respectively. Lamellar-type precipitates were recognized dominantly in T6 specimen while large numbers of small particle-type precipitates were diffused in T5 specimen. To identify these precipitates, energy-dispersive spectrometer (EDS) analysis was conducted, as shown in Fig. 4. From the EDS result, the precipitates were proved to be β -Mg₁₇Al₁₂ since the chemical composition of Mg and Al was 66.8 and 32.5%, respectively. Yoon et al. (Ref 30) reported that with the increasing aging time, the β -Mg₁₇Al₁₂ precipitates gradually

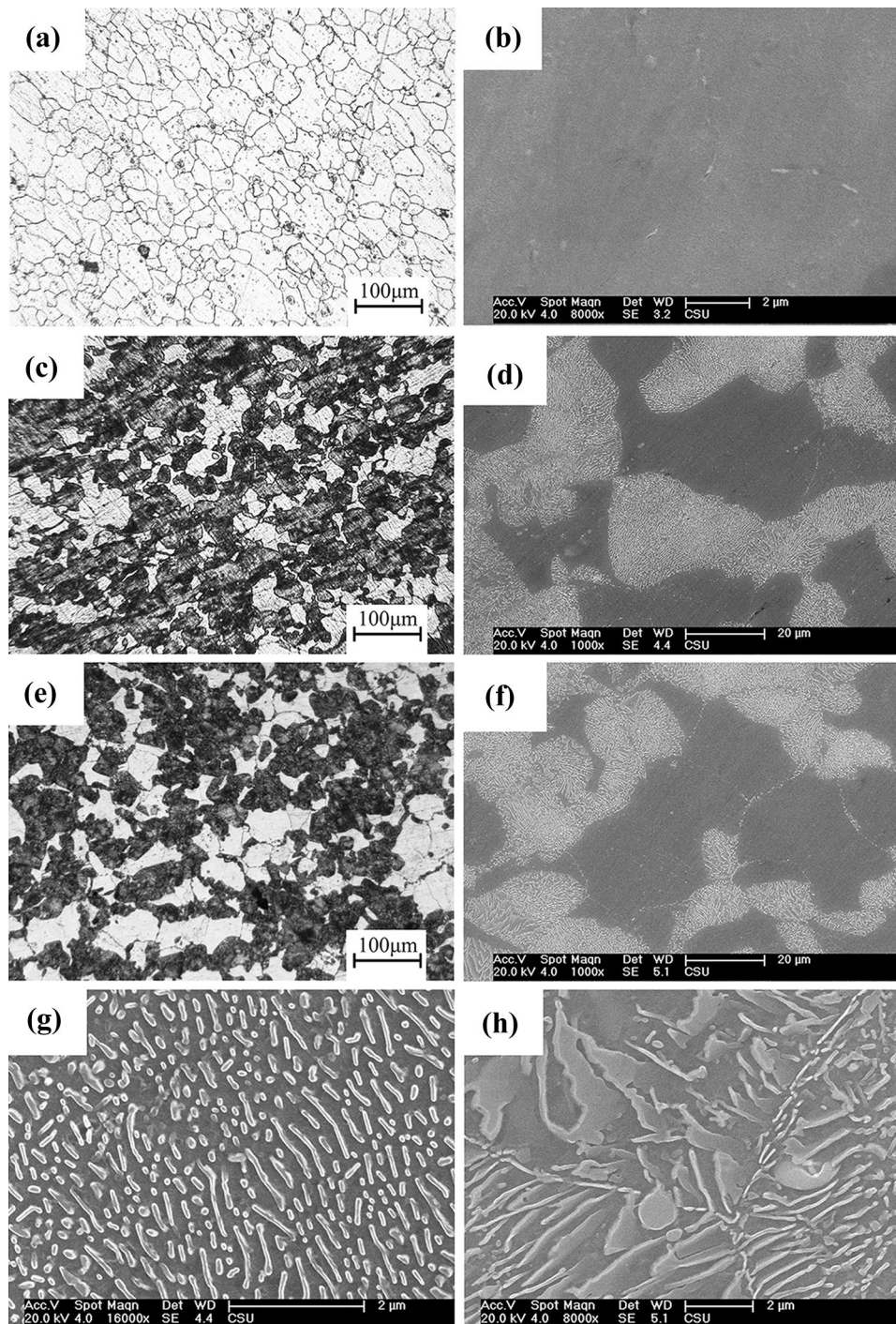


Fig. 3 Microstructures in AZ80: (a) and (b) as-forged, (c) and (d) T5, (e) and (f) T6. The left- and right-side figures depict structures observed by an optical microscope and SEM, respectively. The magnified views of precipitates photographs: (g) T5, (h) T6

increased on the α -Mg in Mg-8Al-0.5Zn alloys. Braszczyńska-Malik (Ref 29) also reported that at 423 K, AZ91 magnesium separates out discontinuous precipitates, while at 473 K, it separates both discontinuous and continuous precipitates. Figure 5 shows the TEM microstructures of specimens. It also noted that β -Mg₁₇Al₁₂ precipitates were produced by heat treatment.

The engineering stress-strain curves of as-forged, T5, and T6 specimens are shown in Fig. 6. The results of tensile tests at room temperature are listed in Table 1. Two important trends

could be inferred from these plots. First, compared with the as-forged specimen, both the yield strength and ultimate tensile strength of T5 and T6 specimens were significantly improved due to the precipitation strengthening of β -Mg₁₇Al₁₂. Second, the elongation of T5 and T6 specimens was decreased owing to the formation of β -Mg₁₇Al₁₂ and grain growth. Furthermore, T5 specimen showed the highest yield strength with the lowest elongation. These tendencies correlated with the results given in Fig. 9, wherein the hardness of the heat treatment specimen increased rapidly. In Fig. 6, the strain hardening phenomenon is

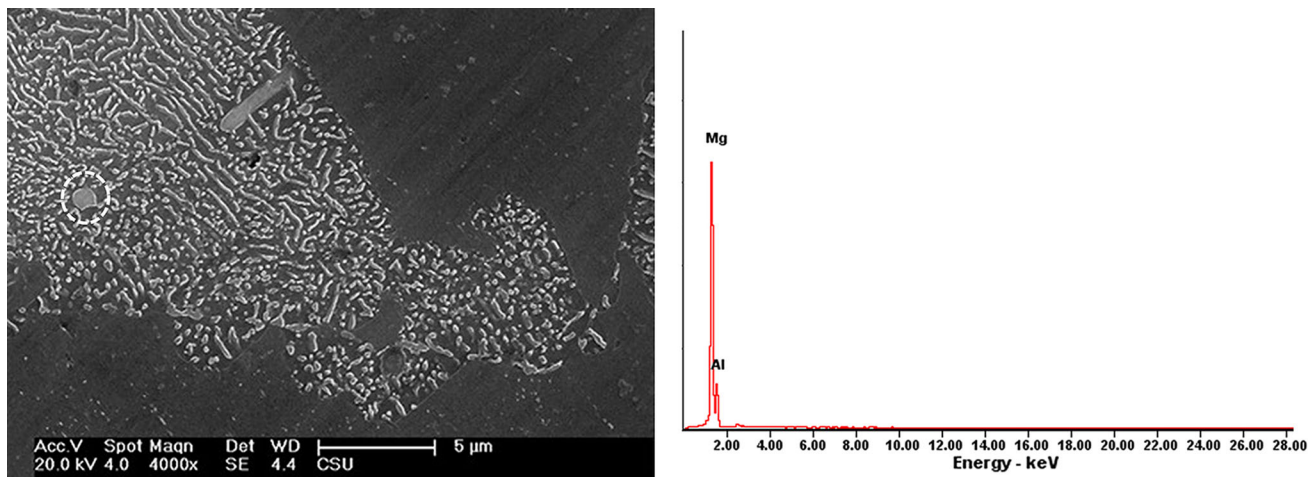


Fig. 4 EDS analysis of precipitates after T5 heat treatment

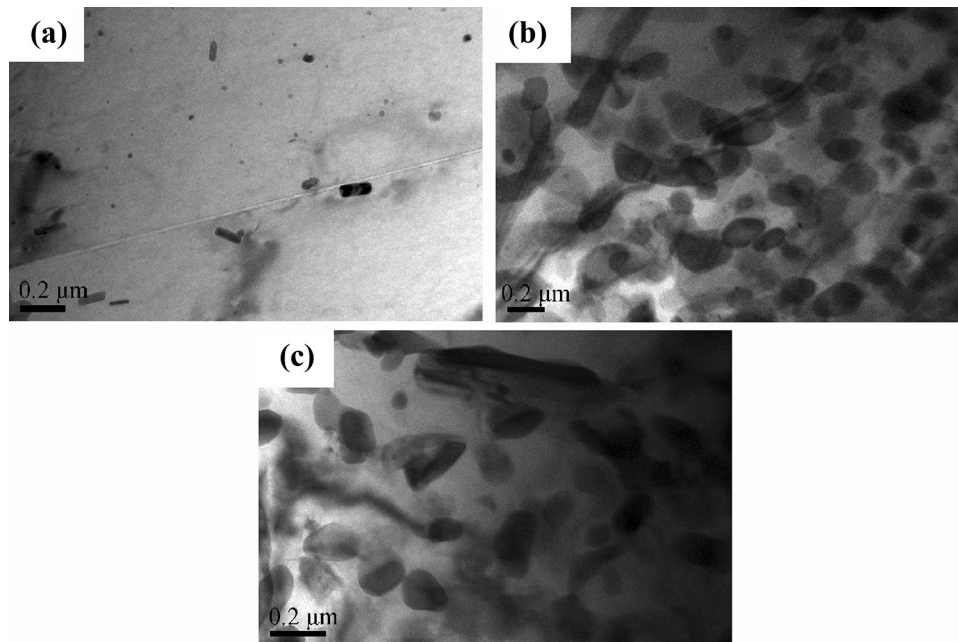


Fig. 5 TEM microstructures of AZ80 alloys: (a) as-forged, (b) T5, (c) T6

observed. These facts indicated that the T5 and T6 heat treatments were effective in improving the mechanical properties of magnesium, which is in agreement with the results of previous reports (Ref 21, 30, 31).

Fracture morphologies of as-forged, T5, and T6 specimens are shown in Fig. 7. The left and right side figures depict fracture surfaces after fracture toughness tests and tensile tests, respectively. The stretched zone (SZ for short) exists between the fatigue pre-crack and fracture surface. The pre-crack propagated direction and the SZ are marked in Fig. 7. Figure 7(a) and (b) shows the fracture surfaces of as-forged

specimen, and many dimples and some cleavage step patterns are presented. On the contrary, the fracture surfaces of T5 specimen (Fig. 7c and d) and T6 specimen (Fig. 7e and f) are shown with many cleavage step patterns and few dimples. Inspection of the fracture surfaces reveals that the as-forged sample show the ductile fracture feature, while the T5 and T6 specimens show brittle fracture feature.

Stretched zone height (SZH for short) analysis has been frequently used to estimate the plane strain fracture toughness, K_{IC} , for thin samples (Ref 8, 9, 11-15). Broek deduced a formula with the relationship between the SZH and the critical

crack tip opening displacement and calculated the value of K_{IC} (Ref 32). Krasowsky and Vainshtok (Ref 33) quantitatively analyzed the relationship between stretched zone parameters and fracture toughness of ductile structural steels. Therefore, the SZH analysis can also be used to calculate the value of K_{IC} . In this method, a sine wave alternating load was applied to the specimen having a sharp pre-crack. And the pre-crack itself blunted and moved forward normal to the span of the specimen to produce the SZ with the load. The SZH is closely related to the value of K_{IC} as given in the following equation (Ref 11, 12, 34):

$$K_{IC} = \left\{ \frac{2 \times SZH \times \lambda \times E \times \sigma_{YS}}{(1 - \nu)^2} \right\}^{1/2}, \quad (\text{Eq 1})$$

where SZH is the value of SZH measured by optical surface profiler microscopy, λ is a constant ($=2$) (Ref 35), σ_{ys} is the tensile yield strength (listed in Table 1), E is Young's modulus, and ν is the Poisson ratio ($=42$ GPa and 0.30 (Ref 36) for pure magnesium alloy, respectively). The cross-section profiles of the samples are shown in Fig. 8, indicating the value of SZH. The calculated values of the fracture toughness of the specimen, K , by Eq 1 are listed in Table 2. The calculated values of fracture toughness, K , are lower than the values of K_Q in each sample. Thus, K is accepted as the value of K_{IC} . The values of K_{IC} shown in Table 2 are 17.9, 23.8,

and 21.0 $\text{MPa m}^{1/2}$ in as-forged, T5, and T6 specimens, respectively. Compared with the as-forged specimen, both the K_{IC} values of T5 and T6 specimens were significantly improved. Moreover, K_{IC} value of T5 specimen was higher than that of T6 specimen due to the diffusion of small particle-type $\beta\text{-Mg}_{17}\text{Al}_{12}$ precipitates and the smaller grain size. It was easy to illustrate that the fracture toughness of as-forged sample could be improved by heat treatment.

The plastic zone was created ahead of the fatigue pre-crack tip and SZ to avoid fracture occurrence. The plastic zone size was generally dependent on the fracture toughness and was directly measurable in principle by several methods, e.g., preferential etching, through recrystallization measurement of void regions (Ref 37) or micro-hardness measurement (Ref 12, 38). In this study, the micro-hardness measurement was carried out on the cross-section of specimen. The hardness was measured at ten points (100 μm apart) off the origin fracture which was the beginning of fracture region. The hardness as a function of the distance from the origin of fracture for as-forged, T5, and T6 specimens is shown in Fig. 9, where the straight lines indicate the initial hardness values on each material. The initial hardness of as-forged, T5, and T6 specimens was 65.3, 82.1, and 80.1 HV, respectively. The hardness near the SZ was much higher than the initial hardness of each sample, and it decreased gradually from the origin of fracture to rest. It suggested that when stress is applied on the specimen, strain hardening could easily occur in the adjacent rupture region, the plastic zone. It was because of the dislocation piled up at the grain boundary or some precipitates and the dislocation interaction. From Fig. 9, it was easy to find that the T5 specimen exhibited a larger hardening region than the T6 specimen. Similarly, T6 specimen also revealed a larger hardening region than the as-forged one. From the economic point of view, T5 heat treatment is more energy saving and efficient than T6 treatment owing to the reduction of solidification step. And the plastic zone size was sensitive to mechanical properties (Ref 12), such as yield strength and strain hardening exponent.

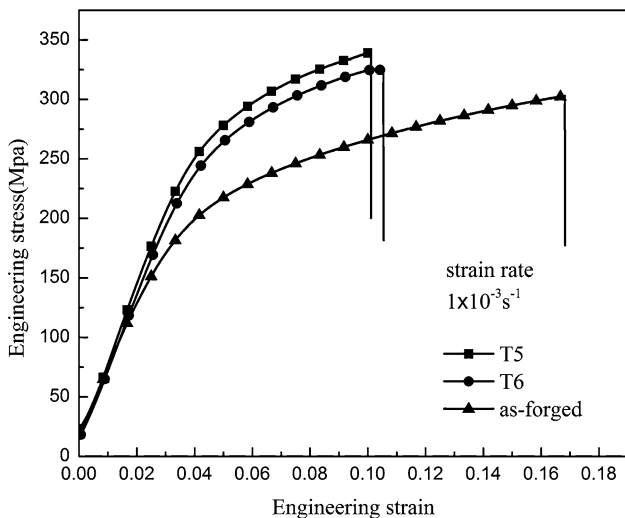


Fig. 6 Engineering stress and engineering strain tensile curve at room temperature of AZ80 alloys

4. Conclusion

In this paper, T5 and T6 heat treatments were applied to the as-forged AZ80 magnesium alloy. The microstructures, XRD, precipitation, and mechanical properties of the alloys under different conditions were investigated to study the effect of heat treatment on fracture toughness at room temperature. The following conclusions can be obtained:

Table 1 The results of tensile tests at room temperature

Material	Tensile yield strength, σ_{ys} , MPa	Ultimate tensile strength, σ_b , MPa	Elongation, δ , %	n
As-forged	194.7	295.8	16.7	0.17
T5	244.3	338.6	10.1	0.33
T6	225.9	325.7	10.5	0.32

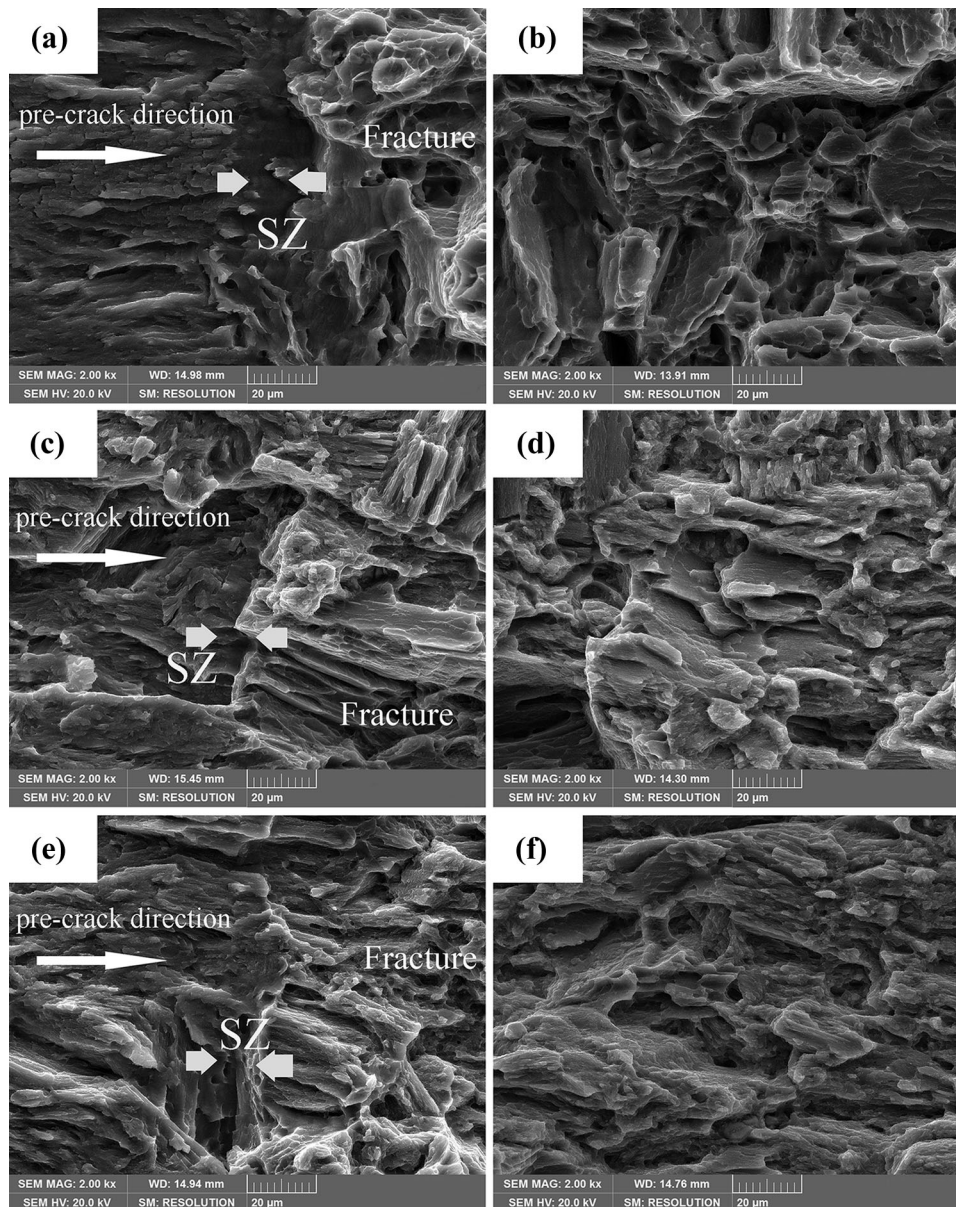


Fig. 7 The fracture surface SEM micrographs of the AZ80 alloys: (a) and (b) as-forged, (c) and (d) T5, (e) and (f) T6. The left- and right-side figures are the fracture surfaces after the plane strain fracture toughness tests and tensile tests, respectively

- (1) The lamellar-type and particle-type $\beta\text{-Mg}_{17}\text{Al}_{12}$ precipitates separated out after T5 and T6 heat treatments. T5 specimen displayed a grain size ($40.3\ \mu\text{m}$) similar to that of as-forged specimen ($39.3\ \mu\text{m}$) but smaller than T6 specimen ($46.1\ \mu\text{m}$).
- (2) After T5 and T6 heat treatments of the as-forged AZ80 magnesium alloy, there was an obvious improvement in the mechanical properties such as yield strength (YS) and ultimate tensile strength (UTS) at room temperature.

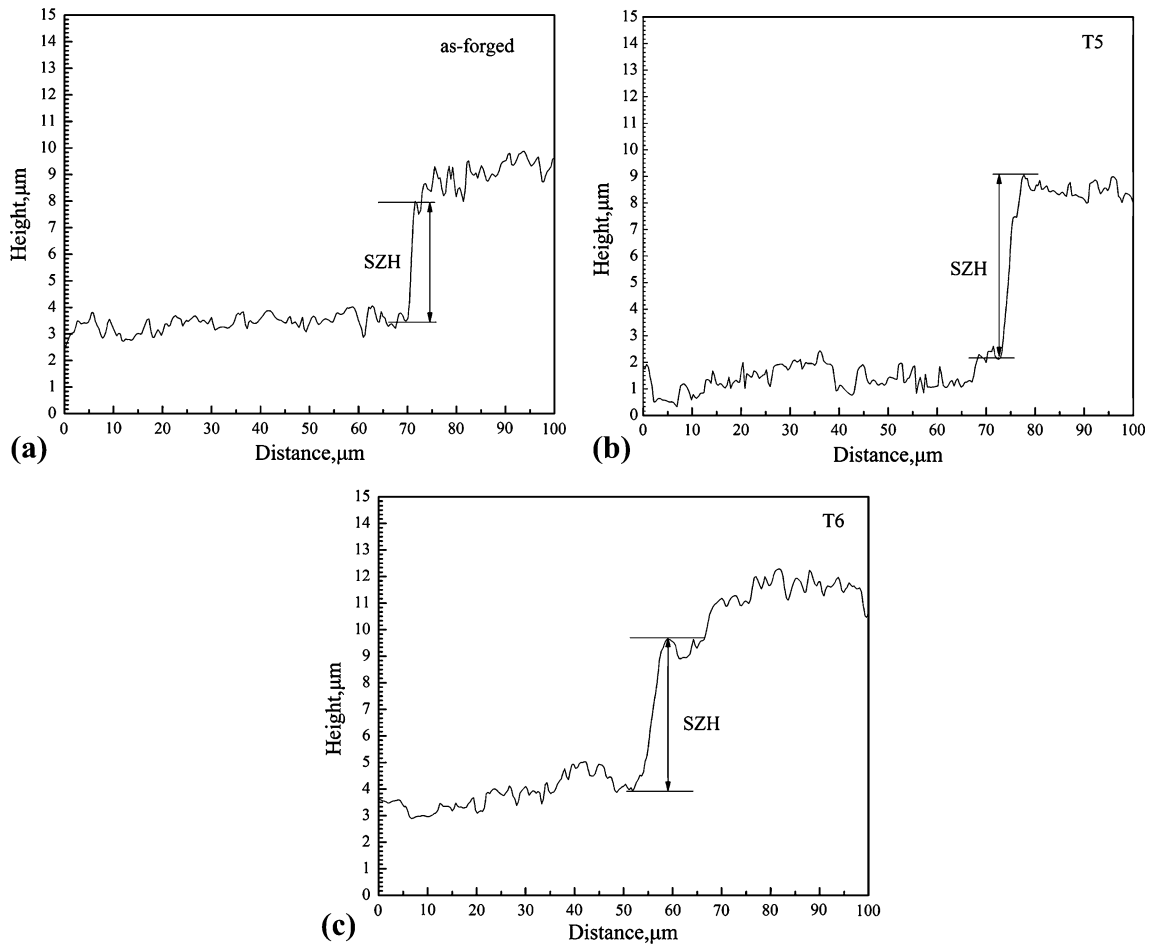


Fig. 8 The cross-section profiles on the surface after plane strain fracture toughness tests: (a) as-forged, (b) T5, (c) T6

Table 2 The results of plane strain fracture toughness tests

Material	SZH, μm	K , $\text{MPa m}^{1/2}$	K_Q , $\text{MPa m}^{1/2}$	K_{IC} , $\text{MPa m}^{1/2}$
As-forged	4.8	17.9	19.2	17.9
T5	6.8	23.8	25.6	23.8
T6	5.7	21.0	23.8	21.0

K is the calculated fracture toughness based on stretched zone height analysis. K_Q is the fracture toughness according to ASTM-E399 and K_{IC} is the plane strain fracture toughness

- (3) The plane strain fracture toughness (K_{IC}) of as-forged specimen was measured to be increased from 17.9 to 23.8 and 21.0 $\text{MPa m}^{1/2}$ after T5 and T6 heat treatments, respectively. And T5 heat treatment is more economical and efficient than T6 treatment.
- (4) The effect of heat treatment on the fracture toughness of as-forged AZ80 magnesium alloy was related to grain size and precipitation of $\beta\text{-Mg}_{17}\text{Al}_{12}$.

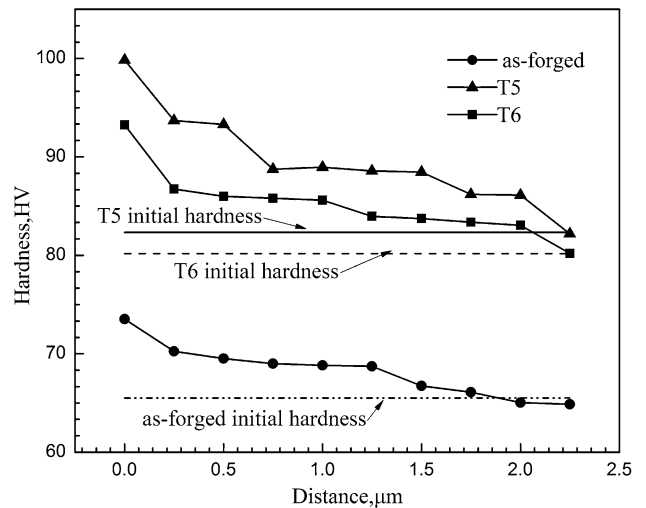


Fig. 9 The hardness as a function of the distance from the origin of fracture on AZ80 alloys

References

1. B.L. Mordike and T. Ebert, Magnesium: Properties—Applications—Potential, *Mater. Sci. Eng. A*, 2001, **302**(1), p 37–45
2. C. Blawert, N. Hort, and K.U. Kainer, Automotive Applications of Magnesium and Its Alloys, *Trans. Indian Inst. Met.*, 2004, **57**(4), p 397–408
3. M. Gupta and N.M.L. Sharon, *Magnesium, Magnesium Alloys, and Magnesium Composites*, Wiley, New York, 2011
4. W. Kasprzak, et al., Correlating Hardness Retention and Phase Transformations of Al and Mg Cast Alloys for Aerospace Applications, *J. Mater. Eng. Perform.*, 2015, **24**(3), p 1365–1378
5. S. Barbagallo and E. Cerri, Evaluation of the K_{IC} and J_{IC} Fracture Parameters in a Sand Cast AZ91 Magnesium Alloy, *Eng. Fail. Anal.*, 2004, **11**(1), p 127–140
6. S. Lee, S.H. Lee, and D.H. Kim, Effect of Y, Sr, and Nd Additions on the Microstructure and Microfracture Mechanism of Squeeze-Cast AZ91-X Magnesium Alloys, *Metall. Mater. Trans. A*, 1998, **29**(4), p 1221–1235
7. K. Purazrang, K.U. Kainer, and B.L. Mordike, Fracture Toughness Behaviour of a Magnesium Alloy Metal-Matrix Composite Produced by the Infiltration Technique, *Composites*, 1991, **22**(6), p 456–462
8. H. Somekawa, A. Singh, and T. Mukai, Effect of Precipitate Shapes on Fracture Toughness in Extruded Mg-Zn-Zr Magnesium Alloys, *J. Mater. Res.*, 2007, **22**(4), p 965–973
9. H. Somekawa, Y. Osawa, and T. Mukai, Effect of Solid-Solution Strengthening on Fracture Toughness in Extruded Mg-Zn Alloys, *Scripta Mater.*, 2006, **55**(7), p 593–596
10. M.F. Ashby, *Materials Selection in Mechanical Design*, 3rd ed., Butterworth-Heinemann, Oxford, 2005, p 58–59
11. H. Somekawa and T. Mukai, Effect of Texture on Fracture Toughness in Extruded AZ31 Magnesium Alloy, *Scripta Mater.*, 2005, **53**(5), p 541–545
12. H. Somekawa and T. Mukai, Fracture Toughness in Mg-Al-Zn Alloy Processed by Equal-Channel-Angular Extrusion, *Scripta Mater.*, 2006, **54**(4), p 633–638
13. H. Somekawa and T. Mukai, Effect of Grain Refinement on Fracture Toughness in Extruded Pure Magnesium, *Scripta Mater.*, 2005, **53**(9), p 1059–1064
14. H. Somekawa, A. Singh, and T. Mukai, Synergetic Effect of Grain Refinement and Spherical Shaped Precipitate Dispersions in Fracture Toughness of a Mg-Zn-Zr alloy, *Mater. Trans.*, 2007, **48**(6), p 1422–1426
15. W.A. Spitzig, A Fractographic Feature of Plane-Strain Fracture in 0.45 C-Ni-Cr-Mo Steel, *ASM Trans. Q.*, 1968, **61**(2), p 344–349
16. T. Sasaki et al., Plane-Strain Fracture Toughness on Thin AZ31 Wrought Magnesium Alloy Sheets, *Mater. Trans.*, 2003, **44**(5), p 986–990
17. G. Eisenmeier et al., Cyclic Deformation and Fatigue Behaviour of the Magnesium Alloy AZ91, *Mater. Sci. Eng. A*, 2001, **319**, p 578–582
18. P. Zhang and J. Lindemann, Influence of Shot Peening on High Cycle Fatigue Properties of the High-Strength Wrought Magnesium Alloy AZ80, *Scripta Mater.*, 2005, **52**(6), p 485–490
19. P. Zhang and J. Lindemann, Effect of Roller Burnishing on the High Cycle Fatigue Performance of the High-Strength Wrought Magnesium Alloy AZ80, *Scripta Mater.*, 2005, **52**(10), p 1011–1015
20. Q. Guo, H.G. Yan, Z.H. Chen, and H. Zhang, Grain Refinement in As-Cast AZ80Mg Alloy Under Large Strain Deformation, *Mater. Charact.*, 2007, **58**(2), p 162–167
21. I.A. Yakubtsov et al., Effects of Heat Treatment on Microstructure and Tensile Deformation of Mg AZ80 Alloy at Room Temperature, *Mater. Sci. Eng. A*, 2008, **496**(1), p 247–255
22. M. Meng et al., Effects of Compression-Pass on Microstructure and Mechanical Properties of AZ80 Alloy, *J. Mater. Eng. Perform.*, 2014, **23**(9), p 3407–3411
23. T. Nakajima, M. Takeda, and T. Endo, Strain Enhanced Precipitate Coarsening During Creep of a Commercial Magnesium Alloy AZ80, *Mater. Trans.*, 2006, **47**(4), p 1098
24. Z.-M. Zhang, H.-Y. Xu, and B.-C. Li, Corrosion Properties of Plastically Deformed AZ80 Magnesium Alloy, *Trans. Nonferrous Met. Soc. China*, 2010, **20**, p s697–s702
25. ASTM E-399, *Standard Test Method for Plane-Strain Fracture Toughness of Metallic Materials*, American Society for Testing and Materials, West Conshohocken, PA, 2001
26. L.V. Chengling et al., Effect of Heat Treatment on Tension-Compression Yield Asymmetry of AZ80 Magnesium Alloy, *Mater. Des.*, 2012, **33**, p 529–533
27. P. Palai et al., Grain Growth and β -Mg₁₇Al₁₂ Intermetallic Phase Dissolution During Heat Treatment and Its Impact on Deformation Behavior of AZ80 Mg-Alloy, *J. Mater. Eng. Perform.*, 2014, **23**(1), p 77–82
28. Z. Yazhe et al., Study on Hell-Petch of AZ80Mg Alloy Under Solution Treatment Condition, *Hot Work. Technol.*, 2013, **42**(2), p 179–181
29. K.N. Braszczynska-Malik, Discontinuous and Continuous Precipitation in Magnesium-Aluminium Type Alloys, *J. Alloys Compd.*, 2009, **477**(1), p 870–876
30. J. Yoon, J. Lee, and J. Lee, Enhancement of the Microstructure and Mechanical Properties in As-Forged Mg-8Al-0.5 Zn Alloy Using T5 Heat Treatment, *Mater. Sci. Eng. A*, 2013, **586**, p 306–312
31. P.C. Wang et al., Effects of T5 Treatment on the Microstructure and Mechanical Properties of Mg-8Al-2Li Alloy, *Mater. Trans. JIM*, 2011, **52**(7), p 1363
32. D. Broek, Correlation Between Stretched Zone Size and Fracture Toughness, *Eng. Fract. Mech.*, 1974, **6**(1), p 173–181
33. A.J. Krasowsky and V.A. Vainshtok, On a Relationship Between Stretched Zone Parameters and Fracture Toughness of Ductile Structural Steels, *Int. J. Fract.*, 1981, **17**(6), p 579–592
34. W.A. Spitzing, Electron Microfractography, *ASTM STP*, 1969, **453**, p 90–109
35. K. Higashi et al., Evaluation of Fracture Toughness of 5083 and 7075 Alloys by Stretched Zone Analysis, *J. Jpn. Inst. Light. Met.*, 1981, **31**, p 720
36. M.M. Avedesian and H. Baker, *Magnesium and Magnesium Alloys*, *ASM Specialty Handbook*, ASM International, Materials Park, OH, 1999
37. C.D. Beachem, T.C. Lupton, and B.F. Brown, A New Technique for Examining Microscopic Fracture Processes at Crack Tips, *Metall. Trans.*, 1971, **2**(1), p 141–143
38. M. Srinivas et al., Ductile Fracture Toughness of Polycrystalline Armco Iron of Varying Grain Size, *Acta Metall. Mater.*, 1991, **39**(5), p 807–816